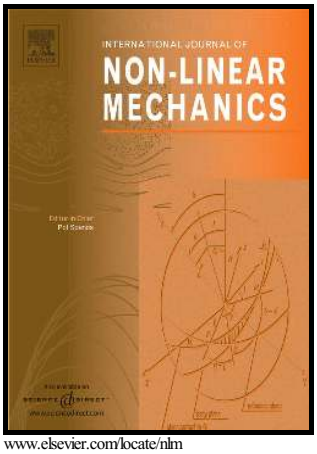

www.elsevier.com/locate/nlm

An investigation of the static and dynamic behavior of electrically actuated rectangular microplates

S. Saghir, M.I. Younis

PII: S0020-7462(16)30059-2
DOI: http://dx.doi.org/10.1016/j.ijnonlinmec.2016.06.004
Reference: NLM2669

To appear in: *International Journal of Non-Linear Mechanics*

Received date: 26 October 2015
Revised date: 3 March 2016
Accepted date: 12 June 2016

Cite this article as: S. Saghir and M.I. Younis, An investigation of the static and dynamic behavior of electrically actuated rectangular microplates, *International Journal of Non-Linear Mechanics* http://dx.doi.org/10.1016/j.ijnonlinmec.2016.06.004

An Investigation of the Static and Dynamic Behavior of Electrically Actuated Rectangular Microplates

S. Saghir, M.I. Younis*

4700 King Abdullah University of Science and Technology (KAUST), Thuwal 23955-6900, Saudi Arabia

* Corresponding author, mohammad.younis@kaust.edu.sa

ABSTRACT

We present an investigation of the static and dynamic behavior of the nonlinear von-Karman plates when actuated by the nonlinear electrostatic forces. The investigation is based on a reduced order model developed using the Galerkin method, which rely on modeshapes and in-plane shape functions extracted using a finite element method. In this study, a fully clamped microplate is considered. We investigate the static behavior and the effect of different non-dimensional design parameters. The static results are validated by comparison with the results calculated by a finite element model. The forced-vibration response of the plate is then investigated when the plate is excited by a harmonic AC load superimposed to a DC load. The dynamic behavior is examined near the primary and secondary (superharmonic and subharmonic) resonances. The microplate shows a strong hardening behavior due to the cubic nonlinearity of mid-plane stretching. However, the behavior switches to softening as the DC load is increased. Finally, near-square plates are studied to understand the effect of geometric imperfections of microplates.

Keywords: electrically actuated microplates, static analysis, dynamics of microplates, diaphragm vibration, large amplitude vibrations, nonlinear dynamics

1. Introduction

Micro-Electro Mechanical Systems (MEMS) commonly use electrically actuated flexible micro-structures, such as microbeams and microplates [1, 2]. Examples include pressure, mass and gas sensors, micropumps, microjets, micromirror, and microphones [3-9]. Modeling accurately the mechanical behavior of such structures under the applied electric force is required to predict the response prior to the experimental testing and actual use of the device. Accurate models can guide the design engineer through the design process; reducing the design time on one hand and on the other hand can help to improve the existing devices. It is common to study the mechanical behavior of MEMS using linear theory [2]; which is applicable only for small deflections. Since in MEMS, structures often undergo large deflection, linear theory becomes inaccurate. Common modeling approaches include lumped mass models and Finite Element Method (FEM) [5, 10-12]. Lumped mass models give rough estimate of the

response only. FEM based software tools are accurate but computationally expensive, especially when it comes to study the nonlinear dynamic behavior. Differential quadrature method (DQM) have been utilized to solve the governing differential equations [13-15]. On the other hand Reduced Order Models (ROM) based on the Galerkin approach have got popularity during the last decades because of their accuracy and low computational cost [16-20]. They have the capability to reveal the effect of different design parameters very conveniently.

In this paper, we present an analytical ROM to study the mechanical behavior of fully clamped microplate based MEMS devices. The model is based on the von-Karman type governing equations of thin plates and is accurate for MEMS devices undergoing geometrically nonlinear large deflections.

A common way to model the plate structures in MEMS devices is using the linear plate theory or classical plate theory (CPT) [6, 21, 22], which is correct when out of plane deflection is small. But in cases when the transverse deflection is comparable to the thickness of the plate, which is very common in MEMS, a strong geometric nonlinearity is present due to mid-plane stretching making the predications of linear theories erroneous.

Machauf et al. [6] studied the characteristics of an electrostatically actuated micropump. They considered the small deflection of a pump diaphragm and used CPT to model the mechanical motion. They applied a sinusoidal voltage across the working fluid and studied the flow rate against different design parameters. W.F. Faris et al [9] presented a model for micropump based on electrostatically actyuated annular members. The model predicts the deflection accurately for any voltage upto the pull-in voltage. Chao and co-workers [21] used the linear plate theory to model the fully clamped thin plate under electrostatic pressure. They employed a reduced order model to develop an analytical expression for the pull in voltage of the flexible thin plate in the applications of microphone and switches. For experimental validation, they designed and fabricated MEMS microphones and found generally good agreement among the theoretical and experimental results. Nayfeh and Younis [22] used the linear plate theory to model the squeeze film damping in microplates. A compressible Reynolds's equation was used to model the squeeze film damping effects. A combination of perturbation and FEM was used to solve for structural modeshapes, the pressure distribution, the natural frequencies, and the quality factors. Theoretically calculated quality factors were found in good agreement with the experimental data.

Ng et al. [5] performed dynamic analysis of microplates under electrostatic forces. They used the boundary element method (BEM) to solve the quasi 3D Laplace equation for the electric potential to calculate the charge density and the corresponding electric force. They modeled the plate using the first order shear deformation theory (FSDT) and employed FEM to discretize the governing equations. Newton's iteration method was used to solve the discretized equations. They compared the results obtained from the FSDT to the results from the linear plate theory and found qualitatively different results. Mukherjee et al. [23] and Telukunta et al. [12] used a fully Lagrangian approach to analyze the coupled electro-mechanical field of microplate based MEMS. They employed FEM for the analysis of mechanical deformations in the plate and the BEM to obtain the electric field exterior to the plate.

Vogl and Nayfeh [18] presented an analytical ROM for fully clamped electrostatically actuated circular plates. The model accounted for the geometric nonlinearity and residual stresses. The governing equations of motion were discretized using the Galerkin approach. The axisymmetric natural frequencies of the plate were determined. Ahmad and Pratap [24] investigated the static response of a clamped circular plate under electrostatic load using the Galerkin method. Bertarelli et al. [25] investigated a circular diaphragm micropump under electric actuation using a one degree-of-freedom analytical model and a finite element model. They analyzed the behavior of the micropump under quasi static and dynamic electric loading. Mohammadi et al. [15] investigated the pull-in instability of electrostatically actuated circular microplates. They used the strain gradient elasticity theory to account for the size effects. A generalized differential quadrature method (GDQ) was used to solve the governing differential equations.

Zhao et al. [17] presented a ROM model for electrostatically actuated rectangular microplates. The model accounted for the nonlinearities due to electric force and mid-plane stretching through the von Karman strains. The Hierarchical Finite Element Method (HFEM) was used to obtain linear undamped mode shapes, which are used in the Galerkin procedure to get a reduced order model. The model was used to calculate the deflection under an applied DC voltage and to study the pull in voltage. Natural frequencies and mode shapes were calculated around the deflected position. Younis and Nayfeh [26] simulated the squeeze film damping of electrically actuated microplates based on the linearized von-Karman plate equations . They used a combination of a perturbation technique and FEM to study the structural mode shapes, the pressure distribution, the natural frequencies, and the quality factors as the DC voltage and air pressure are varied. In addition, some researchers have modeled the thin microstructures as membranes [27, 28]

Zand and Ahmadian [10, 29] investigated the pull-in and vibrational behavior of single and multilayer microplates under electric actuation and squeeze film damping. They used coupled FEM to solve the system of equations. Porfiri [30] investigated the small vibrations of a parallel array of identical microplates deflected under electric loading. They showed that the vibrational properties can be tuned by properly selecting the DC voltage across the adjacent microplates.

Fu and Zhang [31] investigated the active control of the nonlinear static and dynamic responses of piezoelectric viscoelastic microplates actuated electrically. They employed the nonlinear von Karman equations of the plate and used the Galerkin method to reduce the equation. Jia et al. [13] investigated the pull-in instability of electrostatically actuated micro-swtiches including the axial residual stresses. They used Euler–Bernoulli beam theory along with von_Karman type kinematics to formulate the problem and used differential quadrature method to solve the governing equations. Karimzade et al. [32] studied the nonlinear pull-in instability of a fully clamped microplate with movable base. They solved the governing equation using the extended Kantorovich method and the Galerkin approximation technique. Srinivas [33] investigated the static and dynamic pull-in of simply supported microplates using a closed form solution and compared the results with those of a Galerkin approximation.

In recent years, the modified couple stress theory has attracted several researchers for nonlinear analysis of micro structures [34-37]. Gholipour et al. [35] investigated the in-plane and out of plane size

dependent nonlinear dynamics of microplates resting on elastic foundation. Farokhi and Ghayesh [35] investigated the dynamic behavior of geometrically imperfect microplates.

Despite the aforementioned works on the mechanical behavior of microplates; most of the works have been mainly focused on the static and linear vibration behavior of microplates. Almost no work has been presented about the nonlinear behavior of microplates when actuated by large electrostatic loading or when undergoing large motion. Understanding such behaviors is fundamental to the development of the next generation microplates-based MEMS devices.

The objective of this paper is to investigate the nonlinear forced vibration behavior of electrically actuated fully clamped microplates. Towards this, we develop a reduced order model based on the von Karman equations of the plate, in which all three equations of the plate motion are discretized using the Galerkin method. For validation purpose, we compare the static results computed by the reduced order model with the results calculated using the FEM software COMSOL [38]. Further the reduced order model is employed to investigate the dynamic behavior of the plates under large vibration amplitude.

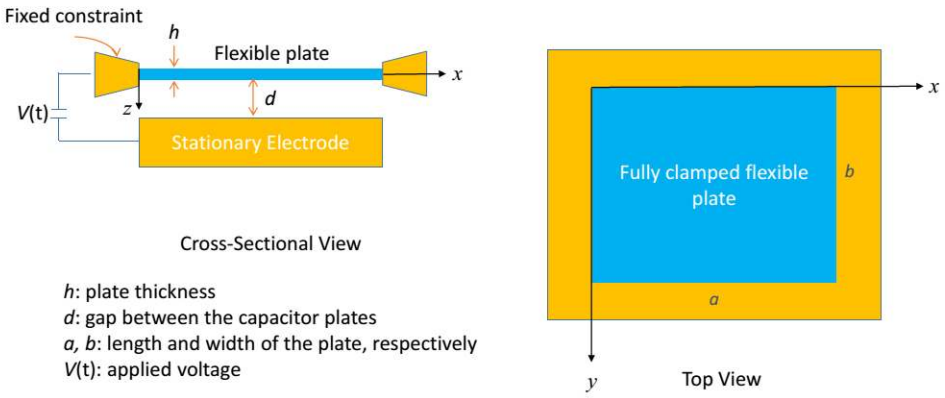

Figure 1: A schematic diagram of an electrically actuated fully clamped microplate.

2. Problem Formulation

We consider a fully clamped rectangular microplate (Figure 1) and adopt the von-Karman equations of motion [39, 40]. We ignore the in-plane inertia since the in-plane natural frequencies are much higher than the transverse natural frequencies. Hence, the in-plane inertia has negligible effect on the transverse motion. Dropping the in plane inertia terms, the governing equations of the plate motion can be written as

$$\frac{\partial^2 u}{\partial x^2}+\frac{1}{2}(1+\upsilon)\frac{\partial^2 v}{\partial x\partial y}+\frac{1}{2}(1-\upsilon)\frac{\partial^2 u}{\partial y^2}+\frac{\partial w}{\partial x}\frac{\partial^2 w}{\partial x^2}+\frac{1}{2}(1+\upsilon)\frac{\partial w}{\partial y}\frac{\partial^2 w}{\partial x\partial y}+\frac{1}{2}(1-\upsilon)\frac{\partial w}{\partial x}\frac{\partial^2 w}{\partial y^2}=0 \quad (1)$$

$$\frac{\partial^2 v}{\partial y^2}+\frac{1}{2}(1+\upsilon)\frac{\partial^2 u}{\partial x\partial y}+\frac{1}{2}(1-\upsilon)\frac{\partial^2 v}{\partial x^2}+\frac{\partial w}{\partial y}\frac{\partial^2 w}{\partial y^2}+\frac{1}{2}(1+\upsilon)\frac{\partial w}{\partial x}\frac{\partial^2 w}{\partial x\partial y}+\frac{1}{2}(1-\upsilon)\frac{\partial w}{\partial y}\frac{\partial^2 w}{\partial x^2}=0 \tag{2}$$

$$\begin{aligned}&\frac{h^2}{12}\nabla^4 w+\frac{\rho(1-\upsilon^2)}{Eh}\frac{\partial^2 w}{\partial t^2}+\frac{c(1-\upsilon^2)}{Eh}\frac{\partial w}{\partial t}=\frac{\varepsilon(1-\upsilon^2)V(t)^2}{2Eh(d-w)^2}+\frac{(1-\upsilon^2)}{Eh}\left(N_{xx}\frac{\partial^2 w}{\partial x^2}+2N_{xy}\frac{\partial^2 w}{\partial x\partial y}+N_{yy}\frac{\partial^2 w}{\partial y^2}\right)\\&+\frac{\partial u}{\partial x}\left(\frac{\partial^2 w}{\partial x^2}+\upsilon\frac{\partial^2 w}{\partial y^2}\right)+\frac{\partial v}{\partial y}\left(\upsilon\frac{\partial^2 w}{\partial x^2}+\frac{\partial^2 w}{\partial y^2}\right)+(1-\upsilon)\left(\frac{\partial u}{\partial y}+\frac{\partial v}{\partial x}\right)\frac{\partial^2 w}{\partial x\partial y}\\&+\frac{1}{2}\left(\frac{\partial w}{\partial x}\right)^2\left(\frac{\partial^2 w}{\partial x^2}+\upsilon\frac{\partial^2 w}{\partial y^2}\right)+\frac{1}{2}\left(\frac{\partial w}{\partial y}\right)^2\left(\upsilon\frac{\partial^2 w}{\partial x^2}+\frac{\partial^2 w}{\partial y^2}\right)+(1-\upsilon)\left(\frac{\partial w}{\partial x}\frac{\partial w}{\partial y}\frac{\partial^2 w}{\partial x\partial y}\right)\end{aligned} \tag{3}$$

where u, v and w are the displacements along the x, y and z direction, respectively, ∇^4 is the bi-harmonic operator $\nabla^4=\frac{\partial^4}{\partial x^4}+2\frac{\partial^4}{\partial x^2\partial y^2}+\frac{\partial^4}{\partial y^4}$, ρ is the mass density per unit area, c is the damping coefficient, and υ and E are Poisson's ratio and modulus of elasticity, respectively. The first term on the right side i.e. $\frac{\varepsilon(1-\upsilon^2)V(t)^2}{2Eh(d-w)^2}$ is the applied electric pressure in the transverse direction while N_{ij} is the applied force per unit length on the edge perpendicular to i^{th} axis in the j^{th} direction.

For convenience, we introduce the non-dimensional variables (denoted by hats);

$$\hat{x}=\frac{x}{a},\quad \hat{y}=\frac{y}{b},\quad \hat{w}=\frac{w}{d},\quad \hat{u}=\frac{au}{d^2},\quad \hat{v}=\frac{av}{d^2},\quad \hat{t}=\frac{t}{T} \tag{4}$$

Substituting equation (4) into equations (1)-(3) and dropping the hats for convenience we get the following equations:

$$\frac{\partial^2 u}{\partial x^2}+\frac{(1+\upsilon)}{2\alpha}\frac{\partial^2 v}{\partial x\partial y}+\frac{(1-\upsilon)}{2\alpha^2}\frac{\partial^2 u}{\partial y^2}+\frac{\partial w}{\partial x}\frac{\partial^2 w}{\partial x^2}+\frac{(1+\upsilon)}{2\alpha^2}\frac{\partial w}{\partial y}\frac{\partial^2 w}{\partial x\partial y}+\frac{(1-\upsilon)}{2\alpha^2}\frac{\partial w}{\partial x}\frac{\partial^2 w}{\partial y^2}=0 \tag{5}$$

$$\frac{\partial^2 v}{\partial y^2}+\frac{(1+\upsilon)\alpha}{2}\frac{\partial^2 u}{\partial x\partial y}+\frac{(1-\upsilon)\alpha^2}{2}\frac{\partial^2 v}{\partial x^2}+\frac{1}{\alpha}\frac{\partial w}{\partial y}\frac{\partial^2 w}{\partial y^2}+\frac{(1+\upsilon)\alpha}{2}\frac{\partial w}{\partial x}\frac{\partial^2 w}{\partial x\partial y}+\frac{(1-\upsilon)}{2}\frac{\partial w}{\partial y}\frac{\partial^2 w}{\partial x^2}=0 \tag{6}$$

$$\begin{aligned}&\frac{\partial^4 w}{\partial x^4}+\frac{2}{\alpha^2}\frac{\partial^4 w}{\partial x^2\partial y^2}+\frac{1}{\alpha^4}\frac{\partial^4 w}{\partial y^4}+\frac{\partial^2 w}{\partial t^2}+\hat{c}\frac{\partial w}{\partial t}=\alpha_2\frac{V(t)^2}{(1-w)^2}+3\alpha_0^2\left\{\hat{N}_{xx}\frac{\partial^2 w}{\partial x^2}+\frac{2}{\alpha}\hat{N}_{xy}\frac{\partial^2 w}{\partial x\partial y}+\frac{1}{\alpha^2}\hat{N}_{yy}\frac{\partial^2 w}{\partial y^2}\right\}\\&+12\alpha_1^2\left\{\frac{\partial u}{\partial x}\left(\frac{\partial^2 w}{\partial x^2}+\frac{\upsilon}{\alpha^2}\frac{\partial^2 w}{\partial y^2}\right)+\frac{1}{\alpha}\frac{\partial v}{\partial y}\left(\upsilon\frac{\partial^2 w}{\partial x^2}+\frac{1}{\alpha^2}\frac{\partial^2 w}{\partial y^2}\right)+(1-\upsilon)\left(\frac{1}{\alpha}\frac{\partial u}{\partial y}+\frac{\partial v}{\partial x}\right)\frac{1}{\alpha}\frac{\partial^2 w}{\partial x\partial y}\right\}\\&+12\alpha_1^2\left\{\frac{1}{2}\left(\frac{\partial w}{\partial x}\right)^2\left(\frac{\partial^2 w}{\partial x^2}+\frac{\upsilon}{\alpha^2}\frac{\partial^2 w}{\partial y^2}\right)+\frac{1}{2\alpha^2}\left(\frac{\partial w}{\partial y}\right)^2\left(\upsilon\frac{\partial^2 w}{\partial x^2}+\frac{1}{\alpha^2}\frac{\partial^2 w}{\partial y^2}\right)+\frac{(1-\upsilon)}{\alpha^2}\left(\frac{\partial w}{\partial x}\frac{\partial w}{\partial y}\frac{\partial^2 w}{\partial x\partial y}\right)\right\}\end{aligned} \tag{7}$$

The parameters appearing in equations (5)-(7) are

$$\alpha=\frac{b}{a},\quad \alpha_0=\frac{a}{h},\quad \alpha_1=\frac{d}{h},\quad \alpha_2=\frac{6\left(1-\upsilon^2\right)}{E h^3 d^3}\varepsilon a^4,\quad \hat{c}=\frac{ca^4}{TD}\quad \text{and}\quad \hat{N}_{ij}=\frac{\left(1-\upsilon^2\right)}{Eh}N_{ij} \tag{8}$$

where $T=\sqrt{\frac{\rho a^4}{D}}$ and $D=\frac{Eh^3}{12\left(1-\nu^2\right)}$

3. Reduced Order Model

To develop the reduced order model for the governing equations (5)-(7), we assume the solution for the transverse and in-plane displacements as follows

$$w=\sum_{i=1}^{n} q_i(t)\phi_i(x,y) \tag{9}$$

$$u=q_u(t)\psi_u(x,y) \tag{10}$$

$$v=q_v(t)\psi_v(x,y) \tag{11}$$

where $\phi_i(x,y)$ are the transversal undamped linear modeshapes of the plate and $q_i(t)$ are the unknown time dependent coefficients, $\psi_u(x,y)$ and $\psi_v(x,y)$ are the shape functions for the in-plane displacements u and v, while $q_u(t)$ and $q_v(t)$ are the corresponding time dependent unknown coefficients.

Since the linear eigenvalue problem governing the transversal undamped linear modeshapes of the fully clamped plate cannot be solved analytically, we resort to the finite element method for this purpose. We use the commercial software COMSOL [38] to obtain the modeshapes of the plate. The in-plane displacement shape functions are also obtained by FEM while the plate is deflected by a uniform transverse pressure. A mesh convergence test is run to choose a suitable mesh. Results of the mesh convergence test and the modeshapes of the plate along with the in-plane displacement shape functions are given in the appendix.

To treat the electric force term we multiply equation (7) by $\left(1-w\right)^2$ so that electric force term is represented exactly [16, 39]. Substituting equations (9)-(11) into equations (5)-(7), multiplying equation (5) and (6) by $\psi_u(x,y)$ and $\psi_v(x,y)$, respectively, and equation (7) by $\phi_i(x,y)$, and integrating over the plate domain, we get a system of differential algebraic equations (DAEs) for the time dependent coefficients. Equations (5) and (6) generate algebraic equations while equation (7) results in ordinary differential equations (ODEs). The resulting system of DAEs is solved for the unknown time dependent coefficients $q_i(t)$, $q_u(t)$ and $q_v(t)$. Toward this, we solve equations (5) and (6) for $q_u(t)$ and $q_v(t)$ in terms of $q_i(t)$ and then substitute the results into equation (7). This equation is then integrated in time

using Runge Kutta. These coefficients are substituted back into equations (9)-(11) to get the displacements w, u and v.

4. Static Analysis

To calculate the static deflection of the microplate under a DC load, we drop the time derivatives in the reduced order model and the time dependent unknown coefficients $q_i(t)$, $q_u(t)$ and $q_v(t)$ are replaced by constant coefficients q_i, q_u and q_v. This results in a system of nonlinear algebraic equations, which is numerically solved for q_i, q_u and q_v. Then equation (9) is used to find the transversal deflection.

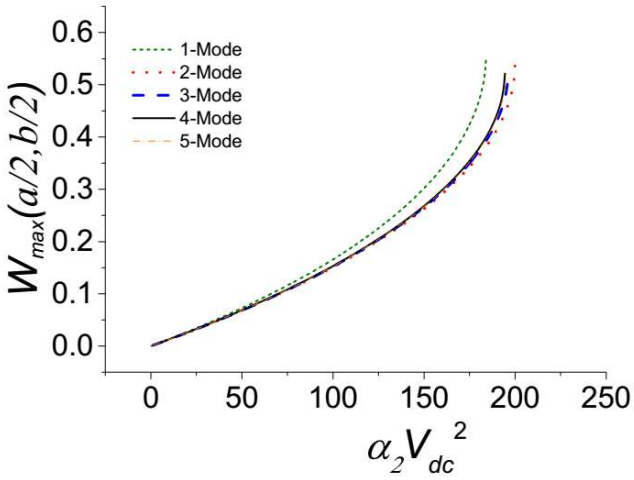

Figure 2: Convergence of the static response with the number of transverse modes retained in the reduced order model. Variation of the maximum non-dimensional deflection $W_{\max}\left(a/2, b/2\right)$ with the electrostatic voltage parameter $\alpha_2 V_{dc}^{\ 2}$ when $\alpha = 1$ and $\alpha_1 = 1$.

First we study convergence of the static results with the number of transverse modes, $\phi_i(x, y)$ retained in the reduced order model when $\alpha = 1$ and $\alpha_1 = 1$.

Figure 2 shows the stable solution, the non-dimensional deflection $W_{\max}$ at the center of plate against various values of $\alpha_2 V_{dc}^{\ 2}$. We note that the static results converge by retaining at least four transverse modes in the model. One can note that the deflection curve is limited by the pull-in instability, where the slope of the curve approaches infinity.

Figure 3 shows the maximum non-dimensional deflection $W_{\max}$ against $\alpha_2 V_{dc}^{\ 2}$ for various values of the aspect ratio α with fixed value of $\alpha_1 = 1$. By increasing α, the maximum deflection almost remains constant, but the voltage instability threshold (pull-in) decreases and saturates near $\alpha_2 V_{dc}^{\ 2} = 75$ as the aspect ratio α approaches ∞.

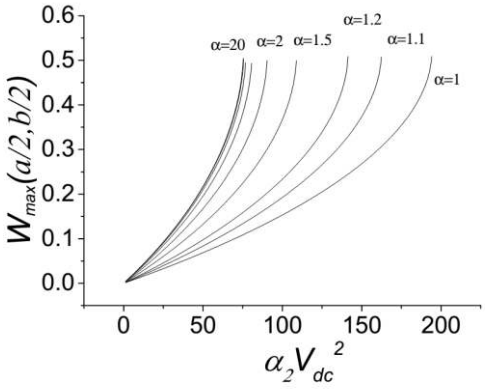

Figure 3: Variation of the maximum non-dimensional deflection $W_{\max}\left(a/2, b/2\right)$ of the microplate with the electrostatic voltage parameter $\alpha_2 V_{dc}^{\ 2}$ until pull-in for various values of aspect ratio α when $\alpha_1 = 1$.

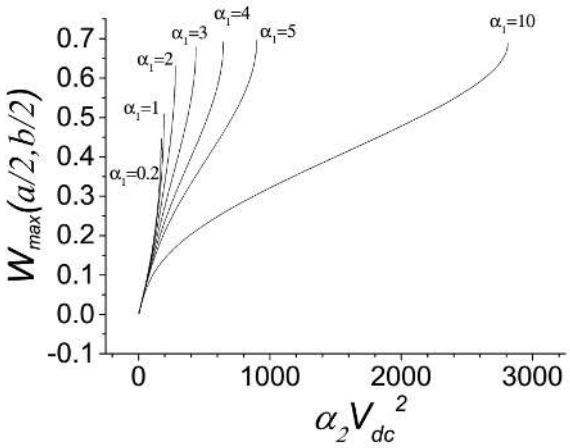

Figure 4: Variation of the non-dimensional deflection $W_{\max}\left(a/2, b/2\right)$ of the microplate with the electrostatic voltage parameter $\alpha_2 V_{dc}^{\ 2}$ until pull-in for various values of α_1 when $\alpha = 1$.

Figure 4 shows the variation of $W_{\max}$ with $\alpha_2 V_{dc}^{\ 2}$ until pull-in occurs for various values of α_1 while $\alpha = 1$ (square plate). We notice that the maximum non-dimensional deflection $W_{\max}$ as well as the voltage parameter $\alpha_2 V_{dc}^{\ 2}$ are reduced for $\alpha_1 < 1$, while for $\alpha_1 > 1$ both quantities increase and $W_{\max}$ seems to stabilize near 0.7 at $\alpha_1 \geq 3$.

5. Model Validation

We validate the reduced order model by comparing its results with the results obtained by FEM software COMSOL [38] for different aspect ratios α. Figure 5 shows the maximum deflection $W_{\max}$ at the center of the microplate calculated by both models. We use rectangular microplates of four different aspect ratios of $\alpha = 1, \alpha = 1.1$, $\alpha = 1.2$, and $\alpha = 1.5$. Dimensional specifications of the electrically actuated microplates are given in Table 1, while material properties are; $E = 153\text{GPa}$ and $\upsilon = 0.23$. Results are shown for various values of V_{dc}, until the pull in instability, for $\alpha = 1.5$. It shows excellent agreement among the results calculated by the ROM model and the FEM model.

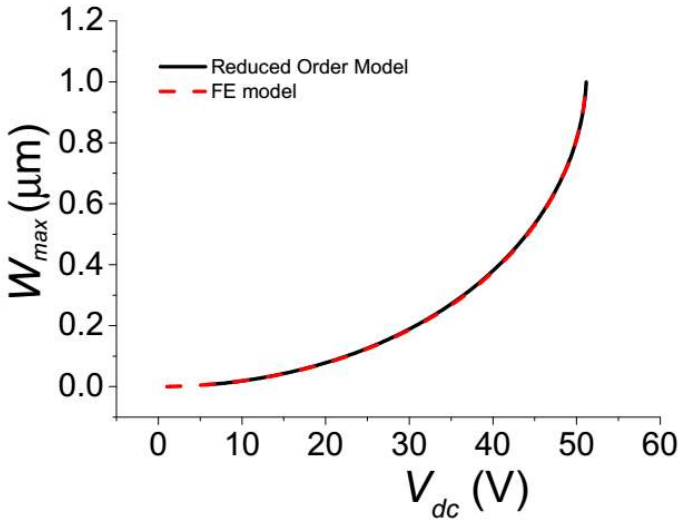

Figure 5: Comparison of the maximum deflection $W_{\max}\left(a/2, b/2\right)$ of the microplate, calculated by the reduced order with the results obtained from FEM for various values of applied DC load V_{dc} until the pull-in instability, for a rectangular microplate of aspect ratio $\alpha = 1.5$.

Table 1: Dimensional specifications of electrically actuated microplates used in the model validation.

Aspect ratio $\alpha = b/a$	Length $a(\mu m)$	Width $b(\mu m)$	Plate thickness $h(\mu m)$	Capacitor gap $d(\mu m)$
1	300	300	2	2
1.1	300	330	2	2
1.2	300	360	2	2
1.5	300	450	2	2

6. Dynamic Analysis

In this section we investigate the dynamic response of the square microplate at primary, super-harmonic of order three and sub-harmonic of order two, resonances of the fundamental mode. We analyze the dynamics of the microplate by generating frequency response curves. The Runge Kutta

method is used to perform long time numerical integration to solve the system of DAEs. The stable steady solution is captured after making sure that the transient response is no longer contributing to the response. Figure 6 shows the time history of the dynamic response of the microplate when actuated at a DC voltage $V_{dc} = 3\text{V}$ and an AC voltage $V_{ac} = 0.1\text{V}$ and $\Omega = 35.1$. Figure 6a depicts the diminishing transient response, while Figure 6b shows the stable steady response. We use steady-state responses similar to Figure 6b to construct the frequency response curves.

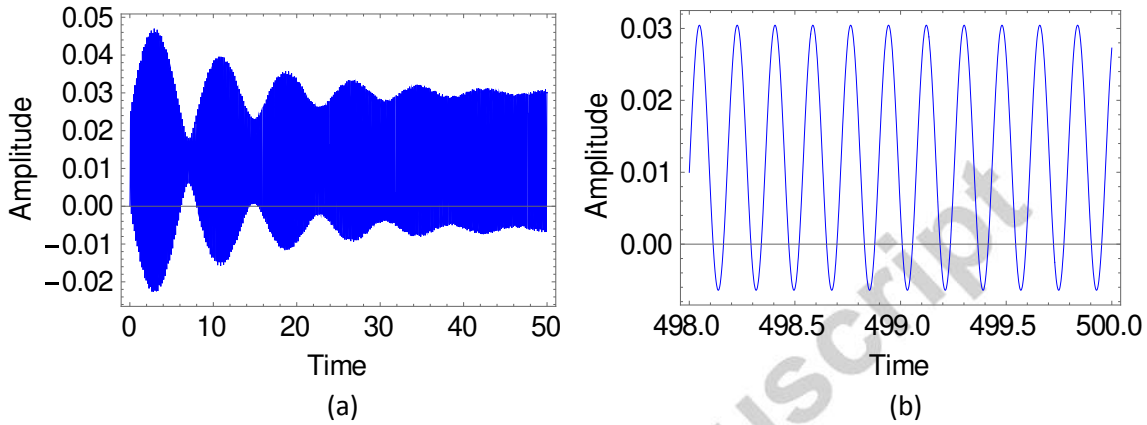

Figure 6: Time history response of the microplate. (a) Transient response. (b) Steady state response.

6.1 Primary Resonance

To investigate the dynamic response at primary resonance, we fix $\alpha = 1$, $\alpha_1 = 1, \alpha_2 = 1$ and assume that the in-plane external forces are zero i.e. $N_{xx} = N_{xy} = N_{yy} = 0$. With the above parameters the static pull-in voltage for the microplate is near 14 Volts. We investigate the nonlinear dynamic behavior of the microplate near primary resonance at a DC voltage superimposed to a small harmonic V_{ac} i.e. $V(\text{t}) = V_{dc} + V_{ac} Sin(\Omega \text{t})$. Figure 7 shows the nonlinear response of the microplate when actuated at $V_{dc} = 3\text{V}$ for various values of V_{ac} while the quality factor is fixed at $Q = 250$ near primary resonance, which for the linear plate is near 36. Our choice of a constant value of Q means that we assumed negligible effect of squeeze-film damping, which reasonable assumption is assuming that the microplate is placed inside a vacuum chamber and is operated at reduced pressure. Otherwise, squeeze-film damping can have strong effect on the dynamics of microplates and needs to be modeled using Reynolds equation and a structural-fluidic model [24, 26].

Figure 7 shows the maximum non-dimensional deflection $W_{\max}$ at the center of the microplate against the non-dimensional frequency. The microplate exhibits strong hardening effect due to the cubic nonlinearity, which comes into play due to mid-plane stretching. The hysteresis in the curves is captured by performing forward and backward frequency sweeps. Nonlinear resonance peaks occur near $\Omega = 36.15$ for $V_{ac} = 0.1\text{V}$ while it is at $\Omega = 36.6$ for $V_{ac} = 0.3\text{V}$ and $\Omega = 36.9$ for $V_{ac} = 0.5\text{V}$. Further we

notice that there exist multiple stable solutions over some range of frequency and amplitude jumps from higher to lower or lower to higher values depending on the type of frequency sweep.

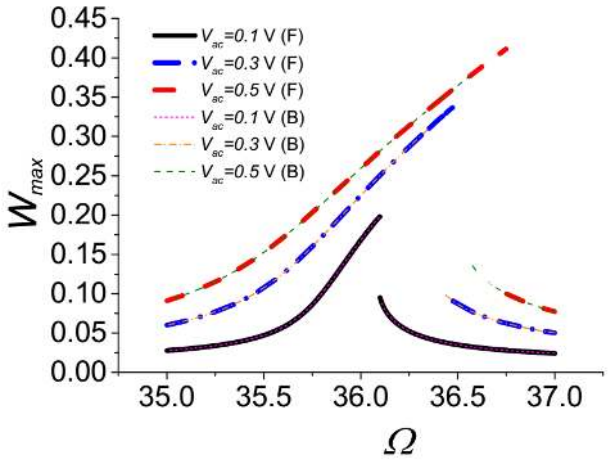

Figure 7: Maximum non-dimensional deflection $W_{\max}\left(a/2, b/2\right)$ of the microplate against the actuating frequency Ω when actuated at $V_{dc}=3\mathrm{V}$ and various values of V_{ac} while quality factor $Q=250$; (F) Forward frequency sweep, (B) Backward frequency sweep.

Figure 8 shows the frequency response curves of the microplate when actuated at $V_{dc}=7\mathrm{V}$ for various values of V_{ac} with a quality factor $Q=250$. An overlap of stable solutions exists when actuated at $V_{ac}=0.2\mathrm{V}$ contrary to the responses at $V_{ac}=0.4\mathrm{V}$ and $V_{ac}=0.6\mathrm{V}$, respectively. A gap between the two stable solutions starts to emerge in the case of $V_{ac}=0.4\mathrm{V}$ by the forward and backward frequency sweeps. This gap might indicate that the microplate becomes unstable at that actuating voltage and pulls on the stationary electrode. This kind of instability is called dynamic pull-in instability, which usually occurs at a lower DC load superimposed to a small harmonic load [39-42]. Another possibility exists, especially in the case of $V_{ac}=0.4\mathrm{V}$, that this gap is created due to the numerical divergence of the time integration scheme, due to its inability to find suitable initial conditions that lead to a stable periodic orbit. In other words, this might indicate highly fractal behavior, which usually gets stronger as the system approaches the dynamic pull-in regime [41]. To confirm if this divergence is due to fractal behavior or due to pull-in exactly, one should resort to other numerical techniques to find periodic motions, such as shooting and finite difference methods as well as basin of attraction analysis [39, 42]. The response on the other hand for the case of $V_{ac}=0.6\mathrm{V}$ is most likely an indication of a pull-in band, since as reported in [42], further increase in V_{ac} widens the pull-in band gap between the stable solutions and makes the upper stable branches terminated at lower values [42].

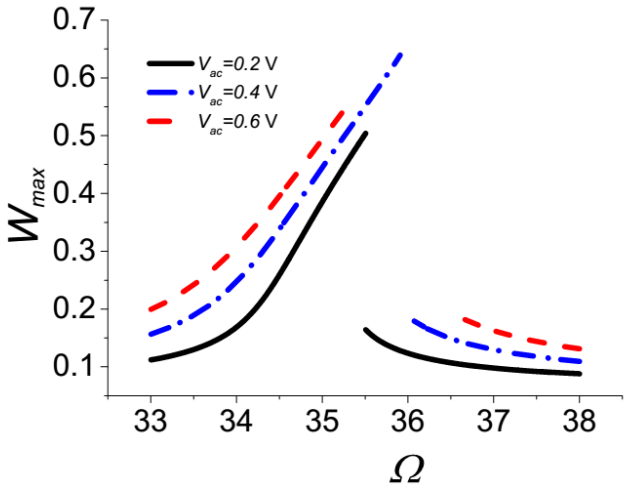

Figure 8: Maximum non-dimensional deflection $W_{\max}\left(a/2, b/2\right)$ of the microplate against the actuating frequency Ω when actuated at $V_{dc}=7\text{V}$ and various values of V_{ac} while quality factor $Q=250$.

6.2 Secondary Resonances

Due to the cubic nonlinearity from mid-plane stretching and quadratic nonlinearity of the electrostatic force, the plate is expected to exhibit several secondary resonances [39, 43]. These include super harmonic resonances near one-third and one-half the fundamental natural frequency as well as subharmonic resonances near twice and three times the fundamental natural frequency. As case studies, in this paper, we investigate the dynamic response of the microplate near the super-harmonic resonance of order three and then near the subharmonic resonance of order half.

A. Super-harmonic Resonance at $\frac{\omega_1}{3}$

We use the same parameters of Section 6.1. The generated frequency response curves reveal some interesting phenomena in this case. First, Figure 9 shows the response at $V_{dc}=9\text{V}$ for various values of V_{ac}. The response at $V_{ac}=2.1\text{V}$ shows a clear hardening behavior. Now increasing the AC voltage to $V_{ac}=2.3\text{V}$ and $V_{ac}=2.4\text{V}$, the microplate becomes unstable and jumps to another stable state with higher amplitude of vibration near $W_{\max}=0.77$. This behavior is contrary to the one near primary resonance where the microplate jumps onto the stationary electrode as dynamic pull-in. This can be due to the fact that the response is in the verge of shifting from hardening to softening effect. This is clarified in Figure 10, which shows the frequency response at $V_{dc}=10\text{V}$ for various V_{ac}. Figure 9 and Figure 10 depict the transition from hardening to softening behavior. This is expected with the increase of the DC voltage, which tends to change the effective nonlinearity of the system. Essentially, the effective nonlinearity is dominated by the mid-plane stretching (positive cubic in nature) for low value of

DC voltage, and thus the plate exhibits hardening behavior. On the other hand, the electrostatic nonlinearities (quadratic in nature) dominate the overall nonlinearities leading to softening behavior at higher values of DC voltage [39, 44]. This observed behavior is expected also for the primary resonance case.

Next, we investigate the amplitude jumps in Figure 9 by plotting phase portraits of the response near terminal points of the lower and upper stable branches. Figure 11 and 12 show the periodic orbits of the stable branches at $V_{ac} = 2.3\text{V}$ and $V_{ac} = 2.4\text{V}$, respectively. Figure 11 shows that the orbit size increases as the actuation frequency increases until the maximum value of deflection amplitude $W_{\max} \approx 0.6$ is reached near the terminal point of the lower stable branch at $\Omega = 11.176$. Beyond this point, we note that the plate jumps to a higher amplitude of vibration, $W_{\max} \approx 0.8$ at $\Omega = 11.178$. The plate jumps back to a lower amplitude of vibration, $W_{\max} \approx 0.27$ at $\Omega = 11.194$. A similar response is depicted in Figure 12 for a higher AC load.

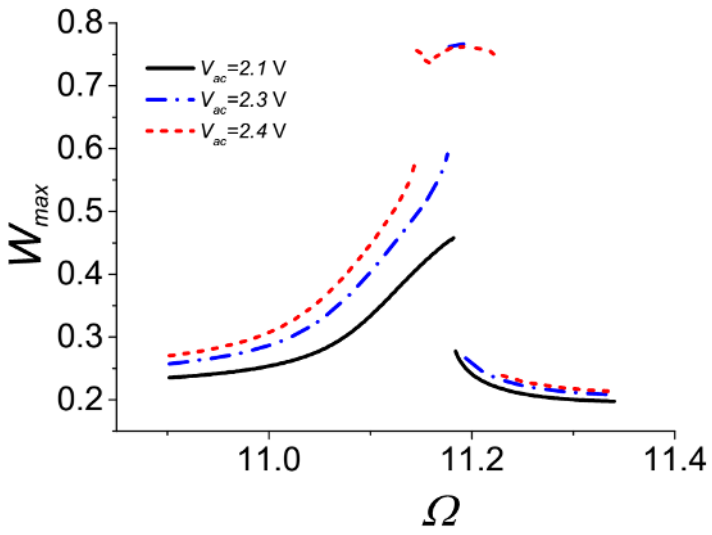

Figure 9: Frequency response curves near super-harmonic resonance, $\frac{\omega_1}{3}$ of the fundamental natural frequency. Maximum non-dimensional deflection $W_{\max}\left(a/2, b/2\right)$ of the microplate against the actuating frequency Ω when actuated at $V_{dc} = 9\text{V}$ and various values of V_{ac} while quality factor $Q = 250$.

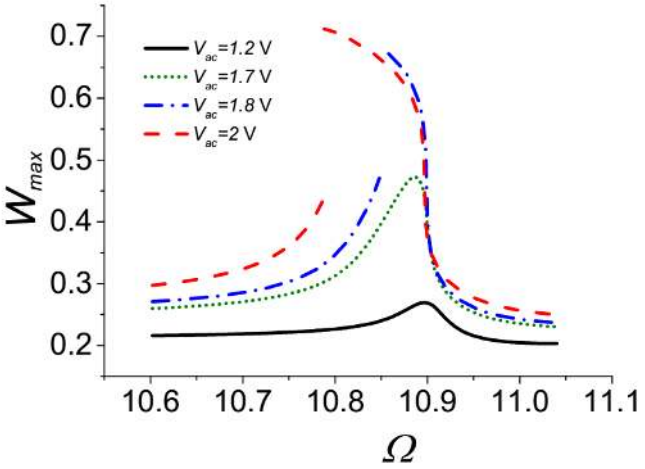

Figure 10: Frequency response curves near super-harmonic resonance, $\frac{\omega_1}{3}$ of the fundamental natural frequency. Maximum non-dimensional deflection $W_{\max}\left(a/2, b/2\right)$ of the microplate against the actuating frequency Ω when actuated at $V_{dc}=10\text{V}$ and various values of V_{ac} while quality factor $Q=250$.

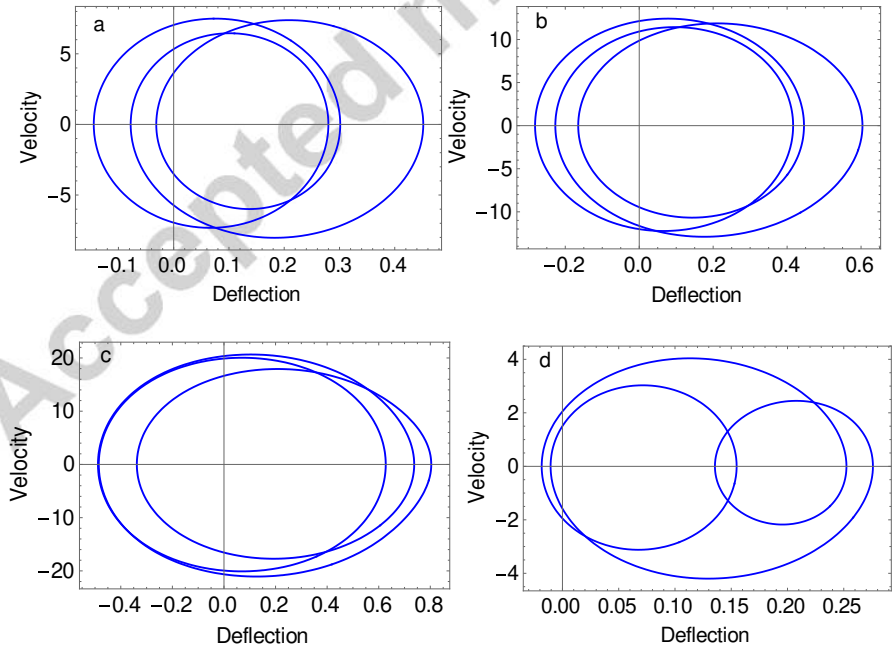

Figure 11: Phase portraits for the lower and upper stable branches of the Figure 9 for $V_{ac}=2.3\text{V}$; (a) $\Omega=11.12$, (b) $\Omega=11.176$, (c) $\Omega=11.178$, (d) $\Omega=11.194$.

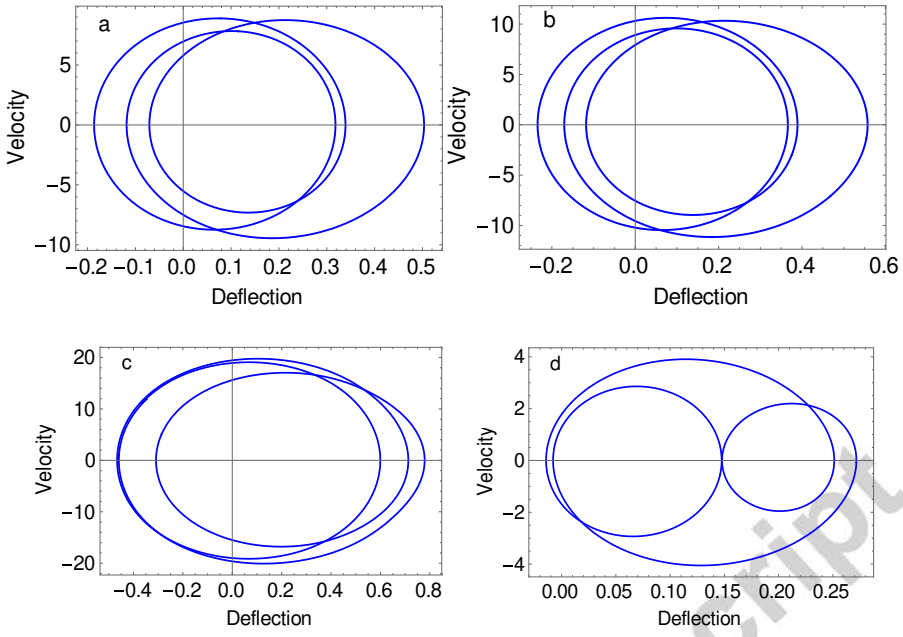

Figure 12: Phase portraits for the lower and upper stable branches of the Figure 6 for $V_{ac} = 2.4\text{V}$; (a) $\Omega = 11.12$, (b) $\Omega = 11.138$, (c) $\Omega = 11.14$, (d) $\Omega = 11.204$.

B. Sub-harmonic Resonance at $2\omega_1$

In this section we investigate the dynamic response of the plate near sub-harmonic resonance of order one half. Figure 13a shows, as expected, a hardening response. This hardening behavior shifts to softening behavior by further increasing the DC voltage. During this transition, Figure 13b, an upper discrete dynamical solution is created of relatively large amplitude (near $W_{\max}$ =0.8), similar to the observed behavior in Figure 9. Figure 13c shows softening behavior at a higher value of DC voltage. The upper stable branch in the case of softening behavior stays high with significantly large amplitude as compared with lower branches for a considerably large band of actuation frequency.

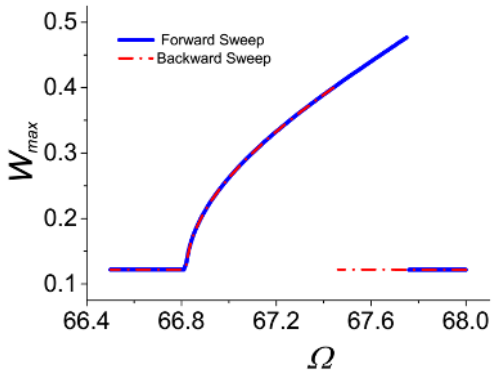

(a) $V_{dc} = 9\text{V}$ and $V_{ac} = 0.5\text{V}$.

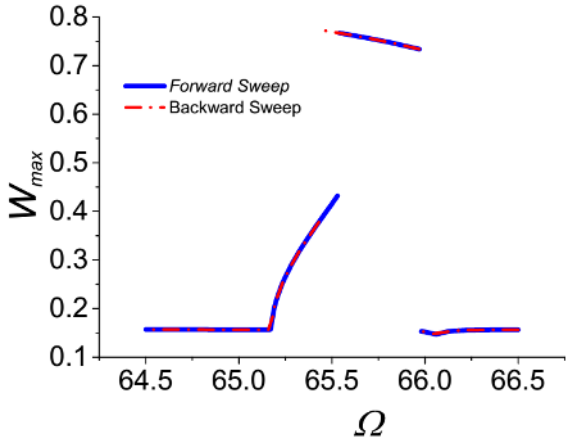

(b) $V_{dc} = 10\text{V}$ and $V_{ac} = 0.5\text{V}$.

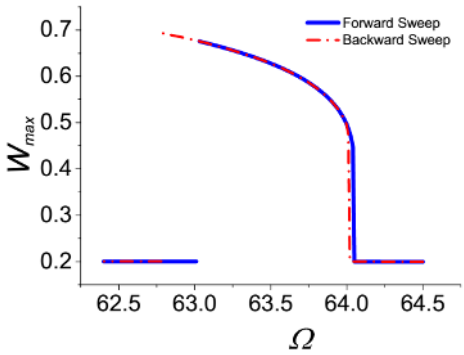

(c) $V_{dc} = 11\text{V}$ and $V_{ac} = 0.5\text{V}$.

Figure 13: Frequency response curves near sub-harmonic resonance near $2\omega_1$. Maximum non-dimensional deflection $W_{\max}\left(a/2, b/2\right)$ of the microplate against the actuating frequency Ω for a quality factor $Q = 250$.

6.3. Dynamic Behavior of Imperfect Square Plates

Next, we investigate the dynamic behavior of imperfect square plates near the second symmetric-symmetric mode, which corresponds to symmetric-symmetric degenerate modes of square plates [45-48]. By imperfect square microplate we mean that α is close to 1. Such an imperfection comes practically when fabricating a square plate, which then due to unavoidable fabrication imperfections, will come as a near square plate. We actuate the microplate at small DC and AC voltages. Non-dimensional parameters remain the same as in subsection 6.1 except α, which we change slightly to introduce the imperfection. A square microplate exhibits degenerate mode due to the symmetrical geometry. Figure 14a shows the response of a perfect square plate i.e. $\alpha = 1$ while Figure 14b-14d shows the responses when α is slightly varied ($\alpha = 0.999$, $\alpha = 0.995$ and $\alpha = 0.99$). It is shown that slightly varying the value of

α breaks the geometrical symmetry and hence the degenerate modes become distinct modes of vibration at distinct frequencies. As a consequence two corresponding resonances appear very close to each other. These neighboring resonances are of interest, for instance, for mass sensing MEMS applications. It is noticed that for very small imperfections the amplitude of the new resonance is very small. By further increasing the imperfection, the amplitudes of both resonances become the same but are smaller than the one with the ideal square plate. This is because we are reducing width of plate (b) while keeping the length (a) constant, to get imperfections, which in return causes higher stiffness of the microplate and hence lower the amplitude of vibration.

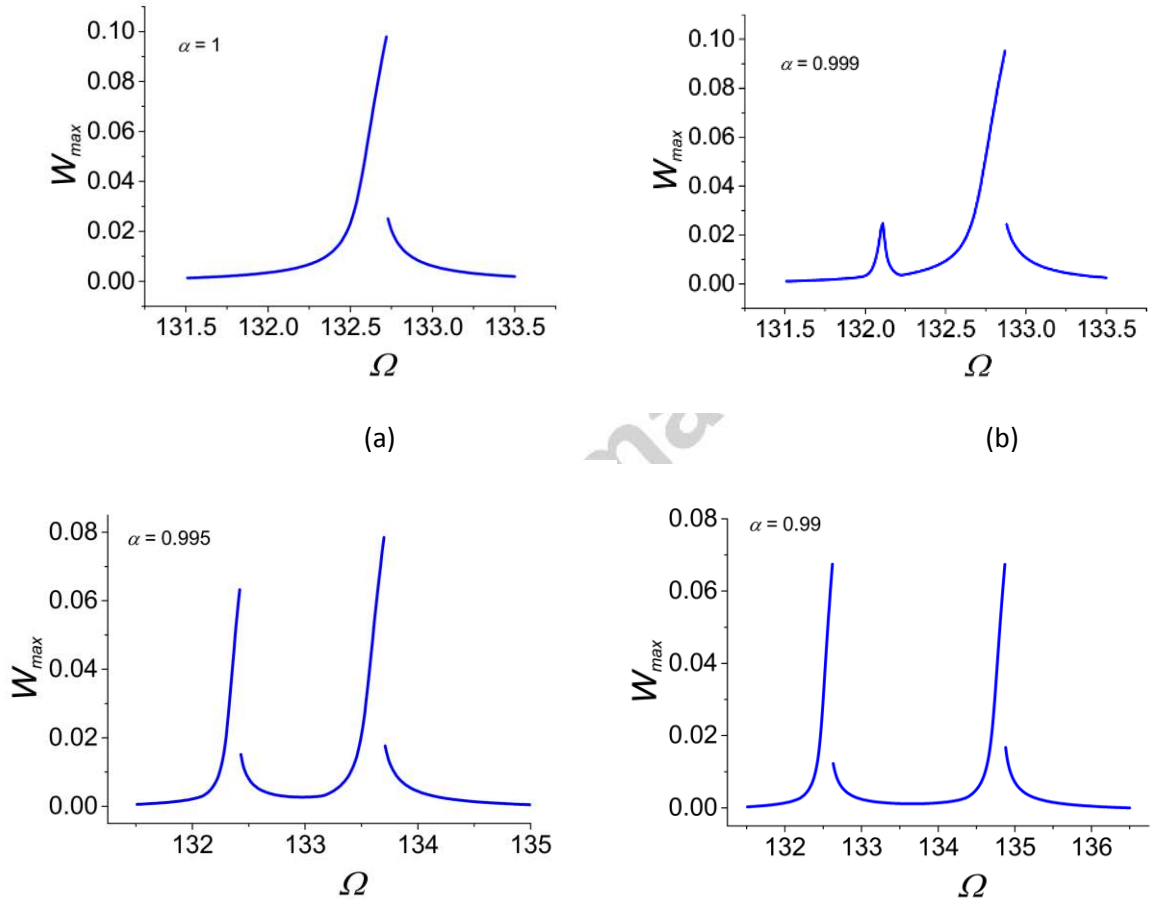

Figure 14: Dynamic behavior of an imperfect square plate near the second symmetric-symmetric mode of vibration when actuated at $V_{dc} = 1\text{V}$, $V_{ac} = 0.3\text{V}$ with a quality factor $Q = 1000$.

6. Conclusions

In this article we developed a reduced order model for the investigation of the static as well as the dynamic behavior of electrically actuated rectangular microplates. First convergence of the static results with the number of modeshapes retained in the ROM has been studied. We found that four modes are sufficient for convergence. We investigated the effect of different non-dimensional parameters on the

static behavior. Increasing the plate aspect ratio α decreases the voltage parameter at pull-in while increasing the gap to thickness ratio α_1 increases the voltage parameter. The dynamic behavior of the microplate has been investigated near primary and super-harmonic resonances using long time numerical integration. We captured the stable solutions using forward and backward frequency sweeps. The microplate actuated near primary resonance shows a strong hardening behavior due to the cubic nonlinearity, which comes into play due to mid-plane stretching. Increasing V_{ac} further widens the gap between the two stable solutions captured by forward and backward frequency sweeps and pull-in instability occurs at a lower vibration amplitude. Interesting phenomena are revealed when the microplate is actuated at $\frac{\omega_1}{3}$ super-harmonic. We found when increasing the applied DC load that there is a transition from hardening behavior to softening behavior. We also investigated the response of imperfect square microplates at the second symmetric-symmetric mode. Breaking the geometrical symmetry by slightly varying the value of α results in distinct neighboring resonances, which can be employed for developing mass sensing MEMS devices.

7. Appendix: Modeshapes and in-plane shape functions

The COMSOL Multiphysics FEM software [38] has been used for the extraction of modeshapes and the in-plane displacement shape functions used in the reduced order model. Towards this, we first performed a mesh convergence test. The FEM model consists of a square plate of side length $100\mu\text{m}$ and thickness of $2\mu\text{m}$. Figure 15 shows the convergence of the first natural frequency with increasing the number of elements. We conclude from the figure that using a mapped mesh with 50 elements along each side of the square microplate is a reasonable compromise between accuracy and computational effort, since further increase of accuracy comes at much higher computational cost.

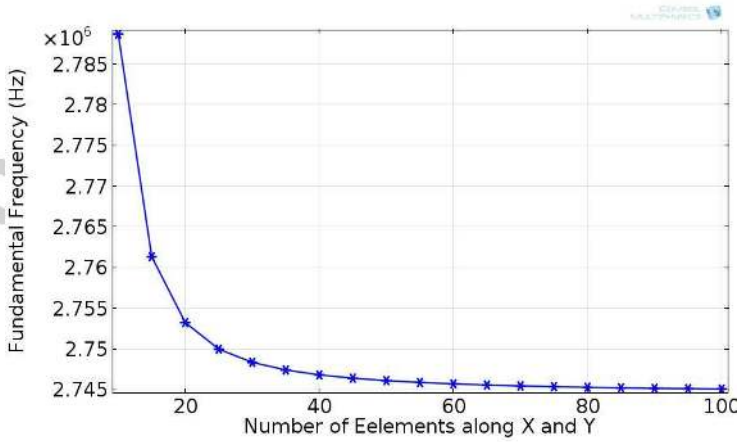

Figure 15: Mesh convergence study; convergence of the first natural frequency with increasing the number of elements.

In Figure 16 we show the in-plane shape functions ψ_u and ψ_v along with the corresponding contour plots. These shape functions are extracted using the FEM software COMSOL [38]. A square microplate is

deflected by applying a uniform transverse pressure. Them the in-plane displacements $u(x,y)$ and $v(x,y)$ are extracted when the deflection at the center of the plate is nearly equal to half the thickness of the microplate. We normalize these displacements to use as shape functions ψ_u and ψ_v for the development of the reduced order model.

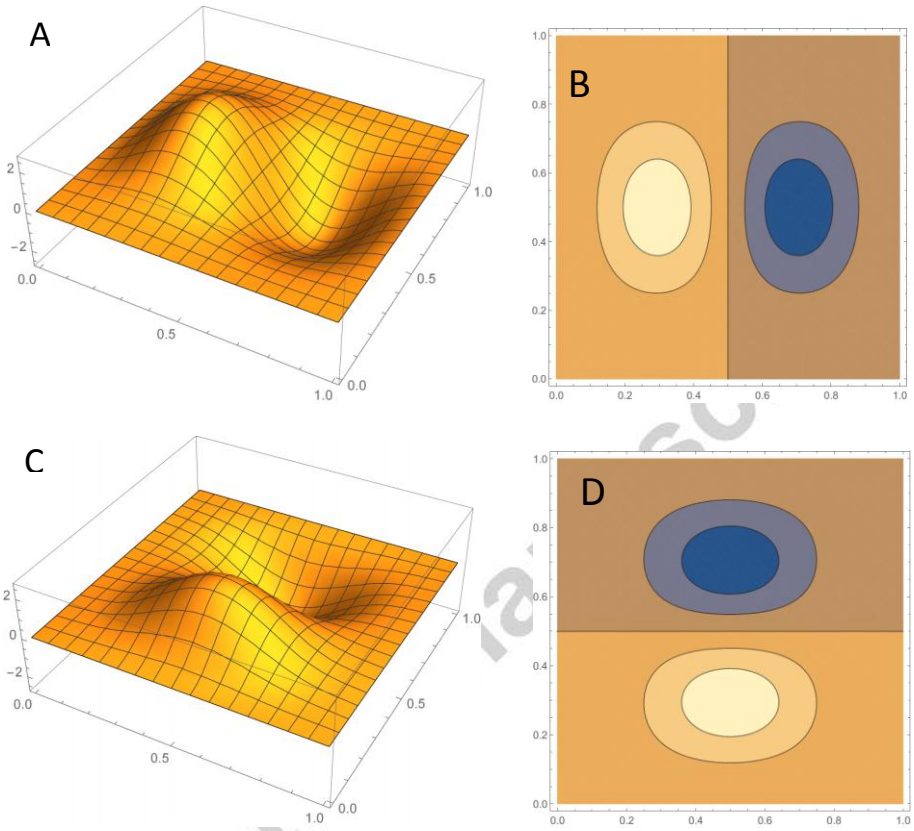

Figure 16: In-plane displacement shape functions, (A) ψ_u plot, (B) ψ_u contour plot, (C) ψ_v plot, and (D) ψ_v contour plot.

The eigenvalue problem of the linear undamped square microplate was solved using the FEM. The first six non-dimensional frequencies, $\lambda = \omega a^2 \sqrt{\frac{\rho}{D}}$, of the symmetric-symmetric modeshapes are provided in Table 2. Figure 17 shows the first six symmetric-symmetric modeshapes used in our model along with corresponding contour plots.

Table 2: Frequency parameter $\lambda = \omega a^2 \sqrt{\frac{\rho}{D}}$ for first six symmetric-symmetric modeshapes of a square microplate calculated using the FEM software COMSOL.

Mode number (ϕ_i)	Non-dimensional frequency parameter $\lambda = \omega a^2 \sqrt{\frac{\rho}{D}}$
ϕ_1	35.89

ϕ_2	130.98
ϕ_3	216.54
ϕ_4	302.87
ϕ_5	383.58
ϕ_6	545.7

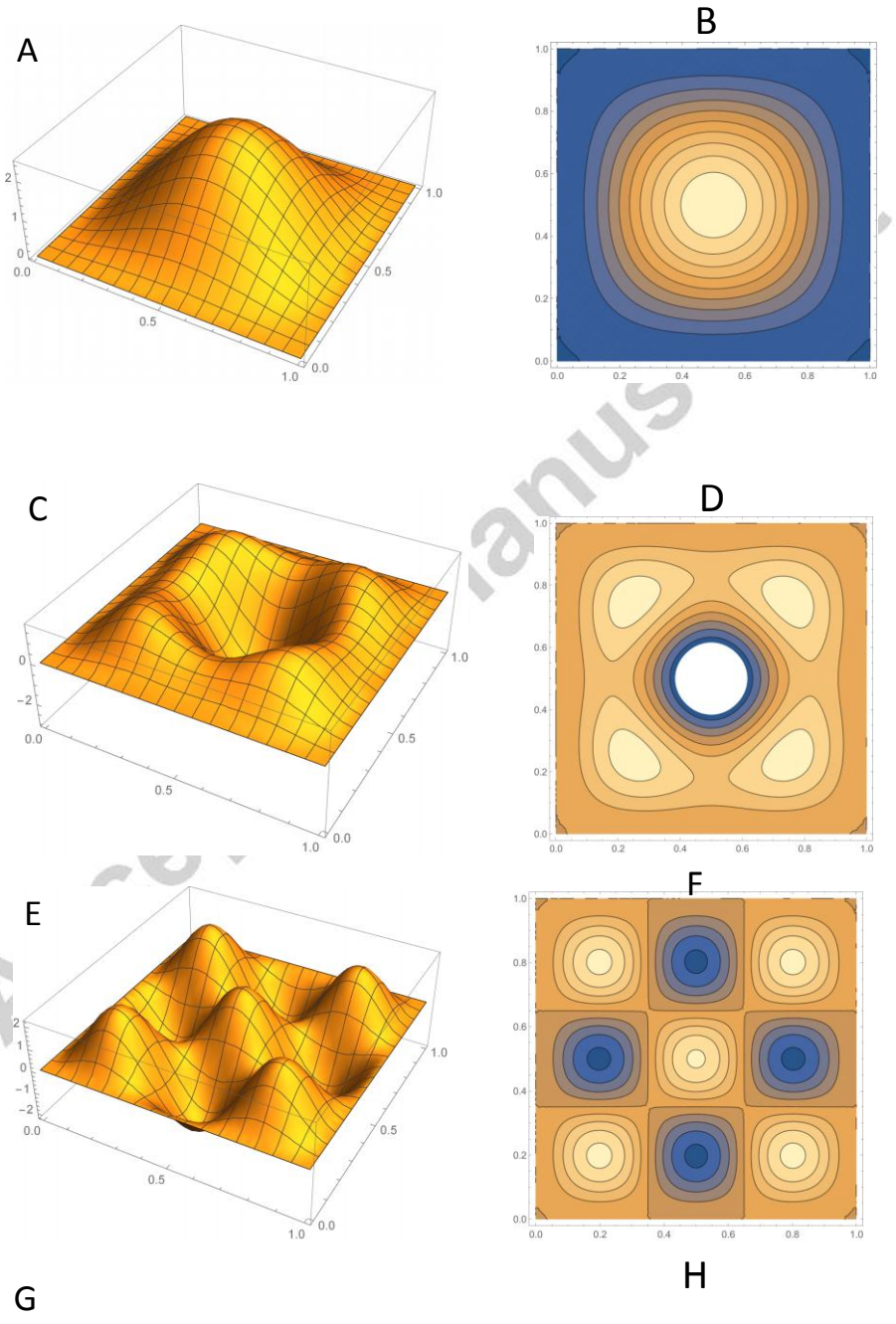

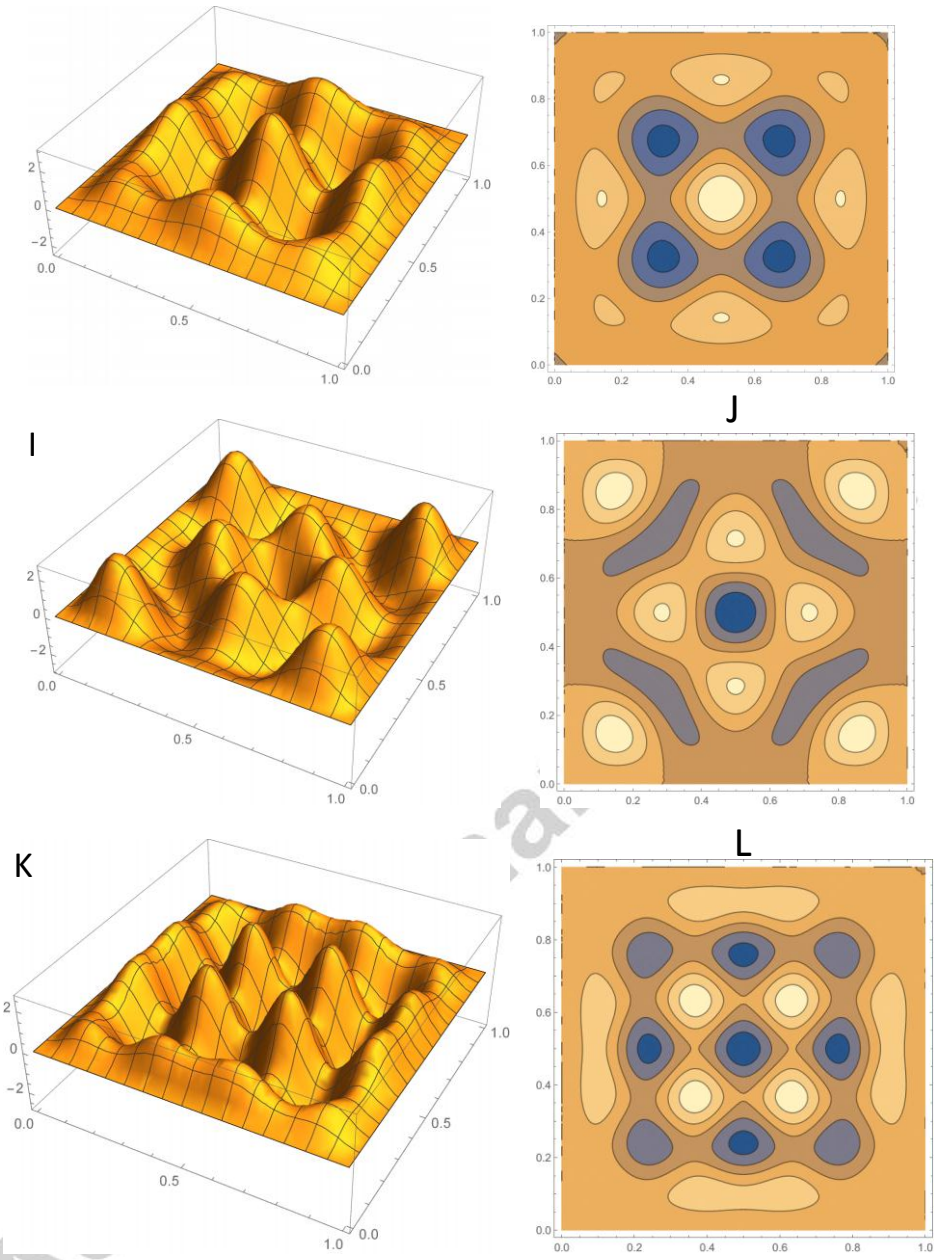

Figure 17: The first six symmetric-symmetric modeshapes of a square microplate (A,C,E,G,I,K) and corresponding contour plots (B,D,F,H,J,L) obtained by an FEM model.

8. References

[1] W.C. Chuang, H.L. Lee, P.Z. Chang, Y.C. Hu, Review on the modeling of electrostatic MEMS, Sensors, 10 (2010) 6149-6171.
[2] R.C. Batra, M. Porfiri, D. Spinello, Review of modeling electrostatically actuated microelectromechanical systems, Smart Materials and Structures, 16 (2007) R23.
[3] P. Tong, W. Huang, Large Deflection of Thin Plates in Pressure Sensor Applications, Journal of Applied Mechanics, 69 (2002) 785-789.

[4] M. Roman, N. Aubry, Design and fabrication of electrostatically actuated synthetic microjets, in: ASME 2003 International Mechanical Engineering Congress and Exposition, American Society of Mechanical Engineers, 2003, pp. 517-524.
[5] T.Y. Ng, T.Y. Jiang, H. Li, K.Y. Lam, J.N. Reddy, A coupled field study on the non-linear dynamic characteristics of an electrostatic micropump, Journal of Sound and Vibration, 273 (2004) 989-1006.
[6] A. Machauf, Y. Nemirovsky, U. Dinnar, A membrane micropump electrostatically actuated across the working fluid, Journal of Micromechanics and Microengineering, 15 (2005) 2309-2316.
[7] S. Horowitz, T. Nishida, L. Cattafesta, M. Sheplak, Development of a micromachined piezoelectric microphone for aeroacoustics applications, The Journal of the Acoustical Society of America, 122 (2007) 3428-3436.
[8] F. Amirouche, Y. Zhou, T. Johnson, Current micropump technologies and their biomedical applications, Microsystem Technologies, 15 (2009) 647-666.
[9] W.F. Faris, E.M. Abdel-Rahman, A.H. Nayfeh, Mechanical behavior of an electrostatically actuated micropump, in: 43 rd AIAA/ASME/ASCE/AHS/ASC Structures, Structural Dynamics, and Materials Conference, Denver, CO, 2002-1303.
[10] M.M. Zand, M. Ahmadian, Characterization of coupled-domain multi-layer microplates in pull-in phenomenon, vibrations and dynamics, International Journal of Mechanical Sciences, 49 (2007) 1226-1237.
[11] A. Pursula, P. Råback, S. Lähteenmäki, J. Lahdenperä, Coupled FEM simulations of accelerometers including nonlinear gas damping with comparison to measurements, Journal of Micromechanics and Microengineering, 16 (2006) 2345-2354.
[12] S. Telukunta, S. Mukherjee, Fully Lagrangian modeling of MEMS with thin plates, IEEE/ASME Journal of Microelectromechanical Systems, 15 (2006) 795-810.
[13] X.L. Jia, J. Yang, S. Kitipornchai, Pull-in instability of geometrically nonlinear micro-switches under electrostatic and Casimir forces, Acta mechanica, 218 (2011) 161-174.
[14] B. Wang, S. Zhou, J. Zhao, X. Chen, Pull-in instability analysis of electrostatically actuated microplate with rectangular shape, International Journal of Precision Engineering and Manufacturing, 12 (2011) 1085-1094.
[15] V. Mohammadi, R. Ansari, M.F. Shojaei, R. Gholami, S. Sahmani, Size-dependent dynamic pull-in instability of hydrostatically and electrostatically actuated circular microplates, Nonlinear Dynamics, 73 (2013) 1515-1526.
[16] M.I. Younis, E.M. Abdel-Rahman, A. Nayfeh, A reduced-order model for electrically actuated microbeam-based MEMS, Microelectromechanical Systems, Journal of, 12 (2003) 672-680.
[17] X. Zhao, E.M. Abdel-Rahman, A.H. Nayfeh, A reduced-order model for electrically actuated microplates, Journal of Micromechanics and Microengineering, 14 (2004) 900-906.
[18] G.W. Vogl, A.H. Nayfeh, A reduced-order model for electrically actuated clamped circular plates, Journal of Micromechanics and Microengineering, 15 (2005) 684-690.
[19] R.C. Batra, M. Porfiri, D. Spinello, Reduced-order models for microelectromechanical rectangular and circular plates incorporating the Casimir force, International Journal of Solids and Structures, 45 (2008) 3558-3583.
[20] A.H. Nayfeh, M.I. Younis, E.M. Abdel-Rahman, Reduced-order models for MEMS applications, Nonlinear dynamics, 41 (2005) 211-236.
[21] P.C. Chao, C.-W. Chiu, C. Tsai, A novel method to predict the pull-in voltage in a closed form for micro-plates actuated by a distributed electrostatic force, Journal of Micromechanics and microengineering, 16 (2006) 986-998.
[22] A.H. Nayfeh, M.I. Younis, A new approach to the modeling and simulation of flexible microstructures under the effect of squeeze-film damping, Journal of Micromechanics and Microengineering, 14 (2004) 170-181.

[23] S. Mukherjee, Z. Bao, M. Roman, N. Aubry, Nonlinear mechanics of MEMS plates with a total Lagrangian approach, Computers & Structures, 83 (2005) 758-768.
[24] B. Ahmad, R. Pratap, Elasto-electrostatic analysis of circular microplates used in capacitive micromachined ultrasonic transducers, Sensors Journal, IEEE, 10 (2010) 1767-1773.
[25] E. Bertarelli, R. Ardito, R. Ardito, A. Corigliano, R. Contro, A plate model for the evaluation of pull-in instability occurrence in electrostatic micropump diaphragms, International Journal of Applied Mechanics, 3 (2011) 1-19.
[26] M.I. Younis, A.H. Nayfeh, Simulation of squeeze-film damping of microplates actuated by large electrostatic load, Journal of Computational and Nonlinear Dynamics, 2 (2007) 232-241.
[27] R.C. Batra, M. Porfiri, D. Spinello, Analysis of electrostatic MEMS using meshless local Petrov–Galerkin (MLPG) method, Engineering Analysis with Boundary Elements, 30 (2006) 949-962.
[28] J. Pelesko, X. Chen, Electrostatic deflections of circular elastic membranes, Journal of Electrostatics, 57 (2003) 1-12.
[29] M.M. Zand, M. Ahmadian, Vibrational analysis of electrostatically actuated microstructures considering nonlinear effects, Communications in Nonlinear Science and Numerical Simulation, 14 (2009) 1664-1678.
[30] M. Porfiri, Vibrations of parallel arrays of electrostatically actuated microplates, Journal of Sound and Vibration, 315 (2008) 1071-1085.
[31] Y. Fu, J. Zhang, Active control of the nonlinear static and dynamic responses for piezoelectric viscoelastic microplates, Smart Materials and Structures, 18 (2009) 095037.
[32] A. Karimzade, H. Moeenfard, M.T. Ahmadian, Nonlinear Analysis of Pull-In Voltage for a Fully Clamped Microplate With Movable Base, in: ASME 2012 International Mechanical Engineering Congress and Exposition, American Society of Mechanical Engineers, 2012, pp. 71-75.
[33] D. Srinivas, Electromechanical Dynamics of simply-supported micro-plates, International Journal of Computational Engineering Research, 2 (2012) 2012.
[34] A. Gholipour, H. Farokhi, M.H. Ghayesh, In-plane and out-of-plane nonlinear size-dependent dynamics of microplates, Nonlinear Dynamics, 79 (2014) 1771-1785.
[35] H. Farokhi, M.H. Ghayesh, Nonlinear dynamical behaviour of geometrically imperfect microplates based on modified couple stress theory, International Journal of Mechanical Sciences, 90 (2015) 133-144.
[36] M.H. Ghayesh, H. Farokhi, Nonlinear dynamics of microplates, International Journal of Engineering Science, 86 (2015) 60-73.
[37] M. Rahaeifard, M. Ahmadian, K. Firoozbakhsh, Vibration analysis of electrostatically actuated nonlinear microbridges based on the modified couple stress theory, Applied Mathematical Modelling, (2015).
[38] COMSOL, http://www.comsol.com/.
[39] M.I. Younis, MEMS Linear and Nonlinear Statics and Dynamics: Mems Linear and Nonlinear Statics and Dynamics, Springer, 2011.
[40] F.M. Alsaleem, M.I. Younis, H.M. Ouakad, On the nonlinear resonances and dynamic pull-in of electrostatically actuated resonators, Journal of Micromechanics and Microengineering, 19 (2009) 045013.
[41] F.M. Alsaleem, M. Younis, L. Ruzziconi, An experimental and theoretical investigation of dynamic pull-in in MEMS resonators actuated electrostatically, Microelectromechanical Systems, Journal of, 19 (2010) 794-806.
[42] A.H. Nayfeh, M.I. Younis, E.M. Abdel-Rahman, Dynamic pull-in phenomenon in MEMS resonators, Nonlinear dynamics, 48 (2007) 153-163.

[43]Nayfeh, A. H. and Younis, M. I. “Dynamics of MEMS resonators under superharmonic and subharmonic excitations,” Journal of Micromechanics and Microengineering, Vol. 15, pp. 1840--1847, 2005.
[44] M. Younis, A. Nayfeh, A study of the nonlinear response of a resonant microbeam to an electric actuation, Nonlinear Dynamics, 31 (2003) 91-117.
[45] A.W. Leissa, Vibration of plates, National Aeronautics and Space Administration ;National Technical Information Service, Washington, Springfield, 1969.
[46] G. Warburton, The vibration of rectangular plates, Proceedings of the Institution of Mechanical Engineers, 168 (1954) 371-384.
[47] G. Caldersmith, T.D. Rossing, Determination of modal coupling in vibrating rectangular plates, Applied Acoustics, 17 (1984) 33-44.
[48] M.D. Waller, Vibrations of free rectangular plates, Proceedings of the Physical Society. Section B, 62 (1949) 277-281.